PHYSICAL REVIEW E **84**, 015101(R) (2011)

Spontaneous motion of a droplet coupled with a chemical wave

Hiroyuki Kitahata,[1,2,*] Natsuhiko Yoshinaga,[3] Ken H. Nagai,[4,†] and Yutaka Sumino[5,‡]

[1]*Department of Physics, Graduate School of Science, Chiba University, Chiba 263-8522, Japan*

[2]*Precursory Research for Embryonic Science and Technology, Japan Science and Technology Agency, Saitama 332-0012, Japan*

[3]*Fukui Institute for Fundamental Chemistry, Kyoto University, Kyoto 606-8103, Japan*

[4]*Division of Advanced Sciences, Ochadai Academic Production, Ochanomizu University, Tokyo 112-8610, Japan*

[5]*Department of Applied Physics, The University of Tokyo, Tokyo 113-8656, Japan*

(Received 13 December 2010; revised manuscript received 24 May 2011; published 13 July 2011)

We propose a framework for the spontaneous motion of a droplet coupled with internal dynamic patterns generated in a reaction-diffusion system. The spatiotemporal order of the chemical reaction gives rise to inhomogeneous surface tension and results in self-propulsion driven by the surrounding flow due to the Marangoni effect. Numerical calculations of internal patterns together with theoretical results of the flow fields at low Reynolds number reproduce well the experimental results obtained using a droplet of the Belousov-Zhabotinsky reaction medium.

DOI: 10.1103/PhysRevE.84.015101 PACS number(s): 82.40.Ck, 47.54.Fj, 47.63.mf, 68.03.Cd

Spatiotemporal patterns are widely seen in living systems; target, spiral, stripe, and dot patterns have been observed at various scales from the interior of a cell to a swarm of cells. Most of studies have focused on patterns at larger scales, which can be successfully reproduced using reaction-diffusion dynamics [1]. In contrast, it is only recently that internal patterns in a single cell have been visualized. These patterns are expected to relate to cellular functions; examples include calcium ions for signal transduction [2], Min proteins for cell division [3], and actin cytoskeltons for mechanical properties [4]. Although pattern formation in a cell is expected to be analyzed in the framework of a reaction-diffusion system, as demonstrated in *in vitro* experiments [3], sufficient understanding of the connection between pattern formation and cellular function is lacking. In this paper we focus motility, as a typical aspect of cellular functions, arising from internal patterns.

Several artificial systems imitating cell motility have been proposed as self-propelled particles [5]. Although no external force is exerted on the particles (a force-free condition), the motion is induced by the asymmetric distribution of an electric field, concentration of chemicals, temperature, and so on. These asymmetric distributions are either *a priori* embedded in the asymmetry of the surface properties of the self-propelled objects [6] or *a posteriori* created by nonlinear effects; motion itself destabilizes a symmetric distribution, for instance, through advective flow [7]. In both cases, however, most studies have focused on motion under steady distributions.

In order to understand the dynamic features of cell motility, a system connecting the dynamic pattern with motion is desirable. In fact, experimental and numerical evidence of chemomechanical coupling in such systems has been demonstrated [8,9]. In this Rapid Communication we propose a theoretical framework for a chemical system exhibiting self-organized patterns, leading to spontaneous motion. We consider that the Marangoni effect is suitable for this purpose as it has been shown to drive an object under force-free conditions by an inhomogeneous interfacial tension arising from a gradient in the chemical concentration [10,11]. In our system, the energy supply and consumption can generate a pattern in a droplet through nonlinear chemical kinetics and the pattern at the interface of the droplet creates inhomogeneous interfacial tension. This generates a flow surrounding the droplet, resulting in motion.

We discuss a spherical droplet of incompressible fluid with a radius of R in another fluid. We consider the Stokes equation under the approximation of low Reynolds number [12]. The unsteady term $\rho\partial_t \mathbf{v}$ is also neglected, where ρ is fluid density. We will justify these assumptions later using experimental values. The concentration of chemical species, which determines the interfacial tension, obeys the reaction-diffusion-advection equation. The sets of governing equations are given by

$$\rho\partial_t \mathbf{v} = -\nabla p + \eta\nabla^2 \mathbf{v} = 0, \tag{1}$$

$$\nabla \cdot \mathbf{v} = 0, \tag{2}$$

$$\partial_t \mathbf{c} + (\mathbf{v}\cdot\nabla)\,\mathbf{c} = \mathbf{F}(\mathbf{c}) + \nabla\,(D\nabla\mathbf{c})\,, \tag{3}$$

where $\mathbf{v}$, p, and η are the flow velocity, pressure, and viscosity of the fluid, respectively. $\mathbf{c}(\mathbf{r})$ is a vector composed of concentrations of chemicals, $\mathbf{F}(\mathbf{c})$ corresponds to the reaction kinetics, and D is a diffusion coefficient.

The flow velocity is coupled with the chemical reaction through interfacial tension at the droplet interface. This coupling is described as a force balance in a tangential direction at an interface [11,13]: $\sigma^{(i)}_{r\theta}|_{r=R} = \sigma^{(o)}_{r\theta}|_{r=R} + (\partial\gamma/\partial\theta)/R$, where σ is the stress tensor and $\gamma(\theta)$ is the interfacial tension profile, which is dependent on $\mathbf{c}$.

For simplicity, we consider only the axisymmetric system schematically shown in Fig. 1(a). Since the boundary condition is given at the droplet interface, it is convenient to set the spherical coordinates so that the droplet is fixed, as shown in Fig. 1(b). We adopt the boundary conditions that

*kitahata@physics.s.chiba-u.ac.jp

†Present address: Department of Physics, Graduate School of Science, The University of Tokyo, Tokyo 133-0033, Japan.

‡Present address: Faculty of Education, Aichi University of Education, Aichi 448-8542, Japan.

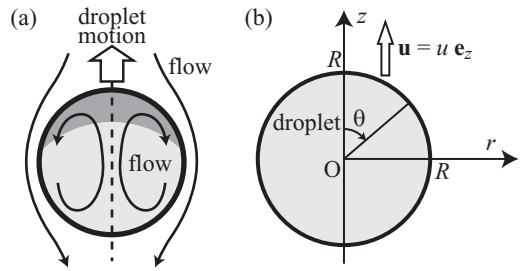

FIG. 1. (a) Schematic representation of the system under consideration. The dashed line corresponds to the symmetry axis. (b) Setting of the coordinates in the droplet system.

$v_r^{(i)} = v_r^{(o)} = 0$ and $v_\theta^{(i)} = v_\theta^{(o)}$ at $r = R$ and $\mathbf{v} \to \mathbf{v}_0 = -\mathbf{u}$ as $r \to \infty$, where r is the distance from the droplet center and $\mathbf{u}$ is the droplet velocity in a laboratory system. The superscripts (i) and (o) correspond to the fluids inside and outside the droplet, respectively. From the symmetric property, we aligned $\mathbf{u}$ with positive z, i.e., $\mathbf{u} = u\mathbf{e}_z$. We also consider the condition that the force exerted on the droplet $\mathbf{f}$ is zero, i.e., $\mathbf{f} = \int dS\, \mathbf{n} \cdot \sigma^{(o)}|_{r=R} = \mathbf{0}$.

By solving Eqs. (1) and (2) with the above conditions, the droplet velocity is calculated as

$$u = -\frac{2}{9\eta^{(i)} + 6\eta^{(o)}}\Gamma_1 \equiv -\alpha\Gamma_1, \tag{4}$$

where Γ_1 is the first-mode coefficient of the Legendre expansion of $\gamma(\theta)$ [13,14] with $\gamma(\theta) = \sum_{n=0}^{\infty} \Gamma_n P_n(\cos\theta)$, where P_n is the Legendre polynominal of order n. The higher modes ($n \geqslant 2$) contribute only to deformation and are independent of the translational motion for small deformation. A detailed derivation of the solution of the Stokes equation is shown in Ref. [15].

We focus on a specific system using the Belousov-Zhabotinsky (BZ) reaction, which is common in experimental systems that can exhibit spatiotemporal pattern formation such as target and spiral patterns in a two-dimensional system [16] and a scroll ring in a three-dimensional system [17]. As a mathematical model for the BZ reaction, we adopt the Oregonator [18], which is widely used due to its reliability, as demonstrated in the physicochemical discussion of the elemental processes of chemical reactions. In the Oregonator, $\mathbf{c}$ is composed of the two variables U and V, which correspond to the concentrations of $HBrO_2$ and an oxidized catalyst, also referred to as the activator and inhibitor, respectively. $\mathbf{F}(\mathbf{c})$ is given by

$$\mathbf{F}(\mathbf{c}) = \mathbf{F}\begin{pmatrix} U \\ V \end{pmatrix} = \begin{pmatrix} \frac{1}{\epsilon}\left(U(1-U) - fV\frac{U-q}{U+q}\right) \\ U - V \end{pmatrix}, \tag{5}$$

where ϵ, q, and f are the parameters that determine the characterisitcs of the BZ reaction. The Oregonator model is nondimensionalized, so the time unit in the calculation is set as T.

The reaction-diffusion-advection equation [Eq. (3)] is numerically solved inside a droplet, which corresponds to the experimental conditions in which a droplet of the BZ reaction medium (the BZ droplet) is inside another fluid. Here, by taking the axisymmetry into consideration, the calculations can be performed in a two-dimensional field. We adopt a monotonically increasing function for the interfacial tension against V:

$$\gamma(V) = \gamma_0 + kV. \tag{6}$$

This assumption is supported by the experimental measurements: The air-water interfacial tension in the ferroin-catalyzed BZ reaction medium is higher in the oxidized state than that in the reduced state [19,20]. In addition, Marangoni flow is observed at the oil-water interface as well as at the air-water interface [8]. Note that the coefficient may include the effect due to the heat generation from the reaction, which only reduces its absolute value.

The parameters for the Oregonator model are set as $q = 0.001$, $\epsilon = 0.05$, and $f = 2.5$, which correspond to the excitable condition, in which a chemical wave propagates only from the initial point. In the numerical calculation, the velocity field is calculated by summing the modes of $n = 1$–8. We confirm that the cut-off modes do not critically affect the numerical results. We perform numerical calculations under two typical sets of conditions: One is a single pulse that corresponds to a target pattern and the other is a scroll ring [17], which is a natural extension of a spiral wave in a three-dimensional medium.

Figure 2 shows the results of numerical calculations for a single pulse. At $t = 0$, a chemical wave is initiated in the lower half of the droplet and then a single chemical wave propagates isotropically. Figure 2 shows snapshots of V in a cross section of the droplet [Fig. 2(a)] as well as the time series of Γ_n ($1 \leqslant n \leqslant 4$) [Fig. 2(b)] and the velocity and position of the droplet [Fig. 2(c)]. The chemical wave arises from the lower part of the droplet and propagates circularly. When the wave reaches the lower boundary of the droplet, the droplet begins

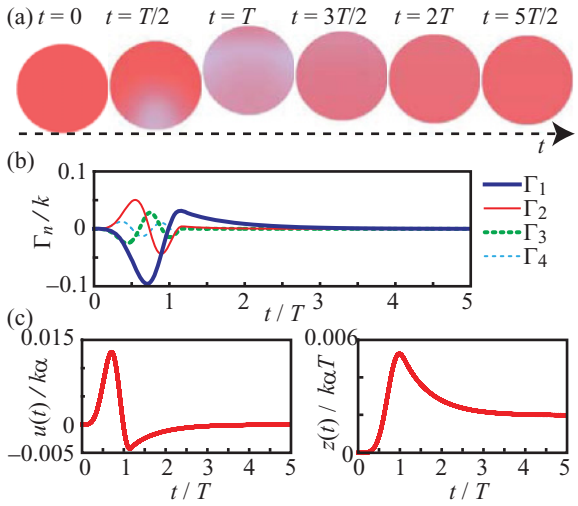

FIG. 2. (Color online) Numerical calculations for a single pulse. (a) Snapshots of V at the cross section and displacement of a droplet. Blue (light gray) and red (dark gray) correspond to higher and lower V, respectively. The displacement is shown as the vertical position. At $t = 0$, a chemical wave was initiated by setting $U = 1$ at a certain region in the lower half of the droplet. (b) Γ_n ($1 \leqslant n \leqslant 4$) plotted against time. (c) Velocity u and the position z of the droplet plotted against time. The parameters $R = 125$ and $D = 1600$.

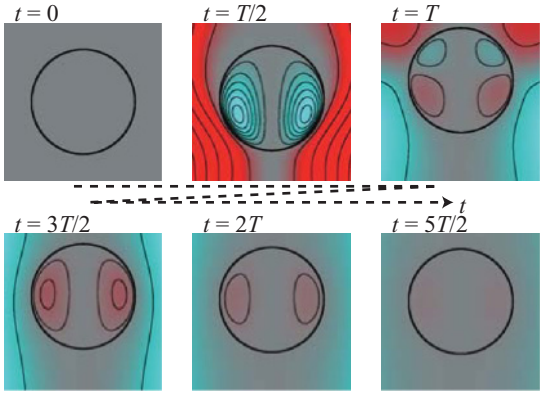

FIG. 3. (Color online) Snapshots of streamlines and stream function at the cross section corresponding to the snapshots in Fig. 2(a). Red (dark gray) and blue (light gray) correspond to positive and negative values of the stream function, respectively [15]. The direction of the rolls in each droplet is shown by red (dark gray) or blue (light gray) [clockwise: red (dark gray) in the left hemisphere and blue (light gray) in the right one; counterclockwise: blue (light gray) in the left hemisphere and red (dark gray) in the right one].

to move upward. When the chemical wave reaches the upper boundary, the droplet moves back in the opposite direction. Nevertheless, there is a net motion in a cycle (see Fig. 2(c) and movies in Ref. [15]). Figure 3 shows snapshots of streamlines in a cross section inside a droplet from the droplet-fixed frame. The direction of the convective rolls is inverted at the moment the droplet moves back.

In the numerical calculation for a scroll ring, the pattern is prepared using the following standard procedure: A chemical wave is first initiated and a part of the chemical wave is omitted by setting U and V as steady-state values at $t = 2.5T$. The numerical results for the snapshots and time series of the position of the droplet are shown in Fig. 4. The droplet moves back and forth, gradually moving upward, coupling with the development of the scroll ring (see the movie in Ref. [15]). In Fig. 4(a) the chemical wave first reaches the lower half of the

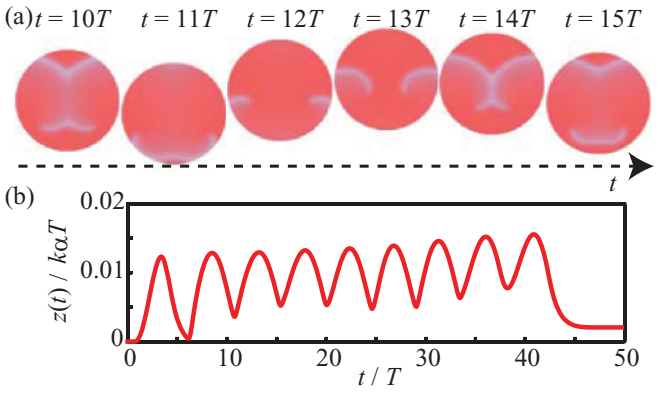

FIG. 4. (Color online) Numerical calculations for a scroll wave. (a) Snapshots of V at the cross section and displacement of a droplet shown in the same manner as in Fig. 2. At $t = 0$, a chemical wave is initiated by setting $U = 1$ at a certain region in the lower half of the droplet and the chemical wave at the central region of the droplet is omitted at $t = 2.5T$. (b) Time series of the position of the droplet. The parameters are $R = 125$ and $D = 60$.

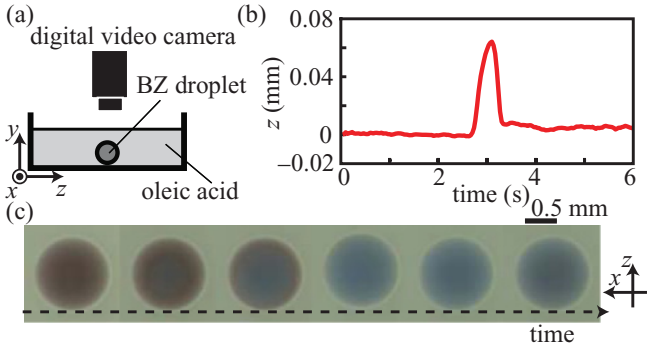

FIG. 5. (Color online) Experiments on the spontaneous motion of a BZ droplet. (a) Schematic representation of the experimental setup. (b) Time change in the center of mass of the BZ droplet. (c) Snapshots in a horizontal plane (x-z plane) every 1 s. Red (dark gray) and blue (light gray) regions correspond to the oxidized and reduced states in the BZ reaction, respectively.

droplet, which leads to upward motion. As the point of contact moves toward the upper half of the droplet, downward motion results. The droplet finally stops since the filament (alignment of the phase singularity points) shrinks and disappears due to its intrinsic instability [21].

In order to compare the theoretical and experimental results, we perform experiments on spontaneous motion of a BZ droplet inside an oil phase, as schematically shown in Fig. 5(a). We put a droplet from the BZ medium with a volume of 1 μl into an oil phase (oleic acid) in a Petri dish made of polytetrafluoroethylene to prevent the droplet from coming into contact with the bottom of the Petri dish. We then observe the BZ droplet from above using a digital video camera (DCR-HC62, Sony, Japan) equipped with a closeup lens (CM-3500, Raynox, Japan). The composition of the BZ reaction medium is $[NaBrO_3] = 0.3M$, $[H_2SO_4] = 0.6M$, $[CH_2(COOH)_2] = 0.1M$, $[NaBr] = 30$ mM, and $[Fe(phen)_3SO_4] = 5$ mM.

The experimental results are summarized in Figs. 5(b) and 5(c). The BZ droplet moves in a horizontal plane. The axis of the position in Fig. 5(b) is set so that the upper direction in Fig. 5(c) is positive. As the BZ reaction medium is prepared under an oscillatory condition, a chemical wave is initiated spontaneously from the point determined stochastically. In Fig. 5(c) a chemical wave is initiated in the lower half of the droplet. When the propagating chemical wave touches the lower interface, the droplet begins to move upward. It then moves back in the opposite direction when the chemical wave propagates over the entire droplet.

From the experimental results, the maximum droplet velocity is measured as $u_{\max} = 0.1$ mm s^{-1}. The viscosity of the BZ medium, $\eta^{(i)}$, is $\sim 10^{-3}$ kg m^{-1} s^{-1} and that of oleic acid, $\eta^{(o)}$, is $\sim 10^{-2}$ kg m^{-1} s^{-1}. The Reynolds number in the present experimental system is calculated with the kinetic viscosity ν as $\mathrm{Re} = uR/\nu \sim 0.1$, which shows that the Stokes approximation is applicable. The relaxation of the velocity field is characterized by $\tau_u = R^2/\nu \sim 1$ s, while the time scale of the wave propagation is $\tau_p = R/\sqrt{D/\epsilon} \sim 1$ s. With these values, we confirm that the time derivative in Eq. (1) does not qualitatively affect our results but modifies Eq. (4) within 15% following the method in Ref. [22]. Therefore, for the sake of simplicity, we assume the flow both inside and

outside the droplet rapidly changes following the changes in chemical concentration. Using these values and the results of the numerical calculations, we estimate the maximum difference in the interfacial tension between the oxidized and reduced conditions as $\Delta\gamma \sim 0.01\ \mathrm{mN\,m^{-1}}$. Although it is difficult to directly measure the interfacial tension at the oil-water interface in this particular system, at an air-water interface of the BZ medium $\Delta\gamma$ is available [20]. The value used in Ref. [20] is ten times higher than our estimation for $\Delta\gamma$ at an oil-water interface. In general, the interfacial tension of an oil-water interface is lower than that of an air-water interface [23] and thus the present estimation seems reasonable.

In summary, we studied droplet motion coupled with internal dynamic pattern formation through an interfacial tension gradient. The Stokes equation was adopted for a spherical droplet and the motion of the droplet was calculated, which reproduced well the experimental results. Although so far we have not experimentally succeeded in generating scrolling rings in a BZ droplet, we expect this motion will be realized by using a photosensitive BZ reaction. A similar model could also be applied to other types of motion, for example, rotational and oscillatory motion. It could be extended further to the motion of a nonspherical droplet.

The authors thank T. Ohta, K. Yoshikawa, M. Sano, H. Kori, and T. Ichino for their helpful discussion. Y.S. and K.H.N. were supported by the Japan Society for the Promotion of Science through Grants No. 21-3566 and No. 23-1819.

[1] K. Matsumoto, S. Takagi, and T. Nakagaki, Biophys. J. **94**, 2492 (2008); S. Kondo and R. Asai, Nature (London) **380**, 678 (1996); J. D. Murray, *Mathematical Biology* (Springer-Verlag, Berlin, 1989); H. Meinhardt and P. A. J. de Boer, Proc. Natl. Am. Soc. **98**, 14202 (2001); J. J. Tyson, K. A. Alexander, V. S. Manoranjan, and J. D. Murray, Physica D **34**, 193 (1989).

[2] J. Keener and J. Sneyd, *Mathematical Physiology* (Springer-Verlag, New York, 1998).

[3] M. Loose, E. Fischer-Friedrich, J. Ries, K. Kruse, and P. Schwille, Science **320**, 789 (2008).

[4] M. G. Vicker, Biophys. Chem. **84**, 87 (2000).

[5] S. J. Ebbens and J. R. Howse, Soft Matter **6**, 726 (2010); W. F. Paxton, S. Sundararajan, T. E. Mallouk, and A. Sen, Angew. Chem. Int. Ed. **45**, 5420 (2006).

[6] W. F. Paxton, K. C. Kistler, C. C. Olmeda, A. Sen, S. K. St. Angelo, Y. Cao, T. E. Mallouk, P. E. Lammert, and V. H. Crespi, J. Am. Chem. Soc. **126**, 13424 (2004); J. R. Howse, R. A. L. Jones, A. J. Ryan, T. Gough, R. Vafabakhsh, and R. Golestanian, Phys. Rev. Lett. **99**, 048102 (2007); H. R. Jiang, N. Yoshinaga, and M. Sano, *ibid*. **105**, 268302 (2010).

[7] F. Domingues Dos Santos and T. Ondarcuhu, Phys. Rev. Lett. **75**, 2972 (1995); Y. Sumino, N. Magome, T. Hamada, and K. Yoshikawa, *ibid*. **94**, 068301 (2005); U. Thiele and E. Knobloch, *ibid.* **97**, 204501 (2006); K. Nagai, Y. Sumino, H. Kitahata, and K. Yoshikawa, Phys. Rev. E **71**, 065301 (2005); M. Nagayama, S. Nakata, Y. Doi, and Y. Hayashima, Physica D **194**, 151 (2004).

[8] H. Kitahata, R. Aihara, N. Magome, and K. Yoshikawa, J. Chem. Phys. **116**, 5666 (2002).

[9] K. Furtado, C. M. Pooley, and J. M. Yeomans, Phys. Rev. E **78**, 046308 (2008).

[10] L. E. Scriven and C. V. Sternling, Nature (London) **187**, 186 (1960).

[11] A. A. Nepomnyashchy, M. G. Velarde, and P. Colinet, *Interfacial Phenomena and Convection* (Chapman & Hall, Boca Raton, 2002).

[12] J. Happel and H. Brenner, *Low Reynolds Number Hydrodynamics: With Special Applications to Particulate Media* (Prentice-Hall, Englewood Cliffs, NJ, 1965).

[13] N. O. Young, J. S. Goldstein, and M. J. Block, J. Fluid Mech. **6**, 350 (1959).

[14] M. D. Levan, J. Colloid Interface Sci. **83**, 11 (1981).

[15] See Supplemental Material at http://link.aps.org/supplemental/10.1103/PhysRevE.84.015101 for solution of the Stokes equation and movies of numerical and experimental results.

[16] R. Kapral and K. Showalter, *Chemical Waves and Patterns* (Kluwer Academic, Dordrecht, 1995).

[17] A. T. Winfree, Science **181**, 937 (1973).

[18] J. P. Keener and J. J. Tyson, Physica D **21**, 307 (1986).

[19] K. Yoshikawa, T. Kusumi, M. Ukitsu, and S. Nakata, Chem. Phys. Lett. **211**, 211 (1993); H. Miike, S. C. Müller, and B. Hess, Phys. Rev. Lett. **61**, 2109 (1988); M. Diewald, K. Matthiessen, S. C. Müller, and H. R. Brand, *ibid*. **77**, 4466 (1996); K. Matthiessen, H. Wilke, and S. C. Müller, Phys. Rev. E **53**, 6056 (1996).

[20] O. Inomoto, K. Abe, T. Amemiya, T. Yamaguchi, and S. Kai, Phys. Rev. E **61**, 5326 (2000).

[21] A. T. Winfree and W. Jahnke, J. Phys. Chem. **93**, 2823 (1989).

[22] V. Galindo, G. Gerbeth, D. Langbein, and M. Treuner, Microgravity Sci. Technol. **7**, 234 (1994).

[23] J. N. Israelachvili, *Intermolecular and Surface Forces* (Academic, London, 1985).